ARTICLES
PUBLISHED ONLINE: 18 MARCH 2012 | DOI: 10.1038/NMAT3278
nature materials

Infrared metamaterial phase holograms

Stéphane Larouche*, Yu-Ju Tsai, Talmage Tyler, Nan M. Jokerst and David R. Smith*

As a result of advances in nanotechnology and the burgeoning capabilities for fabricating materials with controlled nanoscale geometries, the traditional notion of what constitutes an optical device continues to evolve. The fusion of maturing low-cost lithographic techniques with newer optical design strategies has enabled the introduction of artificially structured metamaterials in place of conventional materials for improving optical components as well as realizing new optical functionality. Here we demonstrate multilayer, lithographically patterned, subwavelength, metal elements, whose distribution forms a computer-generated phase hologram in the infrared region (10.6 μm). Metal inclusions exhibit extremely large scattering and can be implemented in metamaterials that exhibit a wide range of effective medium response, including anomalously large or negative refractive index; optical magnetism; and controlled anisotropy. This large palette of metamaterial responses can be leveraged to achieve greater control over the propagation of light, leading to more compact, efficient and versatile optical components.

Diffractive and gradient index (GRIN) optical elements make use of spatial inhomogeneity in the refractive index to focus or otherwise control light. Although both diffractive and GRIN optics bring critical functionality to imaging and spectroscopy beyond what can be achieved with refractive optics, their utility is tempered by the limited contrast of refractive index available from conventional materials and methods of fabrication. On the other hand, these classes of optics naturally lend themselves to artificial structuring, where the effective index range can be broadened by creating subwavelength patterns in otherwise homogeneous dielectric materials, or by varying the relative proportions of two or more dissimilar materials as a function of position. Both of these approaches have achieved increasing relevance owing to the maturation of nanolithographic techniques, which enable ever more sophisticated designs.

There is unquestionably potential for far more advanced and functional optical devices if greater control can be obtained over the underlying materials[1]. Recent developments in transformation optics—a newly appreciated optical design approach—underscore this potential[2]. Transformation optical designs require complex media, often with independent spatial gradients in the tensor elements of the electric permittivity and magnetic permeability throughout the bulk of a medium (that is, three-dimensional, 3D, gradients). Although transformation optical designs are challenging, metamaterial approaches have succeeded in the realization of many optical devices, including approximate versions of invisibility cloaks[3]. Transformation optics has provided the impetus to seek even greater flexibility in material properties.

Although the field of metamaterials is still relatively new, the concept of structuring materials for diffractive and GRIN applications is decades old. Optical filters, for example, often consist of many layers of dielectric materials with nanoscale thicknesses, or continuous index gradients, that are carefully optimized and controlled[4]. To achieve focusing or imaging, however, precise patterning of the material properties must be introduced perpendicular to the optical axis, or even throughout the bulk of a material. Dye diffusion processes have long been employed to achieve GRIN optics in the visible region, but the range of index values for these methods is usually small ($\Delta n \approx 0.05$), with limited spatial index profiles[5,6]. Versatile, direct-write techniques use laser pulses to write arbitrary refractive index distributions inside polymers or glasses, but such methods produce even smaller index variations ($\Delta n \approx 0.01$; ref. 7).

Diffractive optics represents a suitable class of devices for the introduction of artificial structuring, because many diffractive elements are inherently thin and planar lithography can be employed. To a first approximation, control of a wave in a diffractive element is accomplished by controlling the phase of the wavefront as it passes through the layer. The accumulated phase at each point on the emerging wavefront corresponds to the optical path length in the layer traversed by the wave. Control of the optical path length can be achieved in a variety of ways, including changing the amount of material or by changing the refractive index profile as a function of position parallel to the incoming wavefront. With lithographic patterning, multilevel diffractive devices can be formed. The efficiency and performance of such devices, however, suffer owing to the limited number of levels that can be achieved in a reasonable number of fabrication steps.

An important hybrid approach that leverages simple lithographic processing for more efficient diffractive elements is the patterning of subwavelength binary structures. With the application of relatively straightforward effective medium models, collections of subwavelength grooves or pillars can be treated as having effective refractive indices with values that span the range between that of the host dielectric to nearly that of free space[8]. The ability to approach arbitrary index profiles by increasing the number of phase levels translates to substantial improvements to the efficiency and performance of diffractive optics, as has been demonstrated for gratings and computer-generated holograms[9]. However, the feature resolution associated with typical electron beam or optical lithography tends to impose a limit on the number of index levels, and arbitrary index profiles can only be approximated.

Effective medium concepts constitute the core of metamaterial design, in which subwavelength elements provide tailored electromagnetic response. Metal inclusions, in particular, have become key constituents in metamaterial structures, because metals are such strong scatterers of electromagnetic waves. A relatively small, subwavelength, metal inclusion can provide a large electric

Center for Metamaterials and Integrated Plasmonics, Department of Electrical and Computer Engineering, Pratt School of Engineering, Duke University, Box 90291, Durham, North Carolina 27708, USA. *e-mail: stephane.larouche@duke.edu; drsmith@ee.duke.edu.

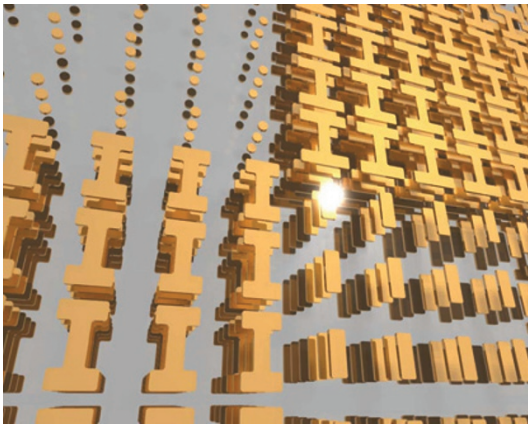

Figure 1 | Artistic rendering of a section of metamaterial hologram demonstrating the various metamaterial elements used in this work. The hologram consists of three layers of gold elements in a SiO_2 matrix over a Ge substrate.

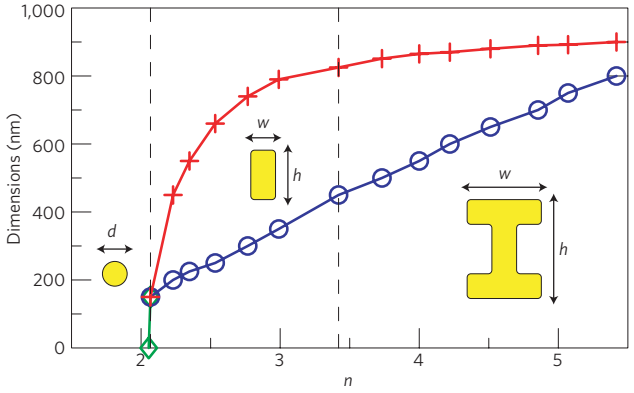

Figure 2 | Relationship between the dimensions of the metamaterial elements and the real part of their effective refractive index. The refractive index is presented for a wavelength of 10.6 μm and for an electric field polarized along the long axis of the rectangular patches, or the axis of the I-beams, the conditions in which the hologram is used. The refractive index is adjusted by controlling the diameter *d* (green diamonds) of circular patches, or the width *w* (blue circles) and height *h* (red crosses) of rectangular patches or I-beams. The refractive index regions covered by the various metamaterial elements are separated by vertical dashed lines. A series of 15 elements or the various types were simulated and their effective refractive index was retrieved (see text for details). Metamaterial elements of intermediate refractive index are obtained by interpolating their dimensions.

polarization, which is extremely sensitive to the size and geometry of the inclusion. By tuning the various parameters of a metal nanoparticle, then, a wide range of refractive index values can be accessed, as well as potentially magnetic response and controlled anisotropy. At microwave frequencies, metamaterials based on resonant, metal elements are now routinely used to form transformation optical media and other complex structures requiring extreme material requirements. In the terahertz regime, for example, extreme refractive index metamaterials have been produced. A lithographically patterned I-beam metamaterial with a refractive index of 33.2 at the resonance frequency of the element has been reported[10]. Such anomalously large refractive index values are complicated by large absorption, but nevertheless illustrate the potential of using metals to access a far greater space of material properties.

In the context of diffractive optics, the sensitivity of metallic elements to their shape and size enables a much finer discretization of index levels, allowing targeted index profiles to be better approximated. However, two major challenges are present when transitioning such metamaterials to optical frequencies: metals are more absorptive, translating into increased absorption in the composite device; and the dimensions of the unit cells are significantly subwavelength and thus require the same sophistication in micro- and nanofabrication techniques used in binary subwavelength structures. Nevertheless, the work presented here shows that it is possible to overcome these challenges and to fabricate a functional holographic device based on a multilayer metamaterial medium with metallic inclusions.

The metamaterials used in this work consist of 75-nm-thick gold discs, rectangular patches or I-beams of various dimensions centred in a 1 μm × 1 μm × 500 nm cuboid of SiO_2. The polarizability of such elements—and therefore the permittivity and the refractive index of the metamaterial—increases with the size of the metallic inclusion. Capacitive coupling between the arms of adjacent I-beams further increases the polarizability of the element when the electric field polarization is parallel to the I-beam axis. Although I-beam metamaterial elements exhibit a circuit-like electrical resonance, where their electromagnetic response peaks, we operate at frequencies away from the resonance frequency to minimize absorption.

Many materials were considered for the metamaterial elements. Whereas gold is one of the best metals at the wavelength of operation, SiO_2 shows significant absorption. However, of all the materials we considered, SiO_2 has the best combination of reasonable losses and process compatibility. A more complete discussion is provided in the Supplementary Information.

A representative set of metamaterial elements used in this work are shown in Fig. 1. The element resulting in the lowest refractive index consists of a gold disc, 150 nm in diameter. Slightly higher refractive indices are obtained using rectangular patches. Finally, the higher refractive indices are obtained using I-beams with a linewidth of 200 nm and varying width and height. For the highest refractive index element, adjacent I-beams are separated by 100 nm gaps. The dimension of the smallest metal patch, the linewidth and the width of the gap of the largest I-beam were all selected to be accessible by the lithographic fabrication process used to create the metamaterial hologram.

Unlike the subwavelength binary structures previously used in diffractive elements, metal metamaterial elements cannot be described using the simpler mixing rules from effective medium theory, where different regions of index contribute roughly by volume to the composite effective index. Instead, the polarization of the metamaterial elements must be computed using full-wave simulations, with the effective properties retrieved by computing the reflection and transmission coefficients and equating these to a homogeneous slab of material[11]. In this work, we modelled a series of 15 distinct elements using Comsol Multiphysics, a commercial, full-wave numerical solver. A normal incidence wave with a free-space wavelength of 10.6 μm was simulated with the electric field polarized along the long axis of rectangular patches or the axis of the I-beams. To more accurately match the fabrication realities, the metallic elements were rounded with a radius of curvature of 30 nm, as estimated from scanning electron microscopy (SEM) images of test samples. Furthermore, all simulations accounted for a 3 nm chromium adhesion layer. The properties of gold are taken from ref. 12, those of chromium from ref. 13 and those of the SiO_2 layer were determined by a point-by-point fit of a set of reflection spectra measured by Fourier transform infrared spectroscopy (Bruker Vertex 80v).

Figure 2 shows the relationship between the extracted refractive index and the dimensions of the metallic elements. By interpolating the physical dimensions of the elements between those modelled, we find that it is possible to obtain arbitrary refractive index

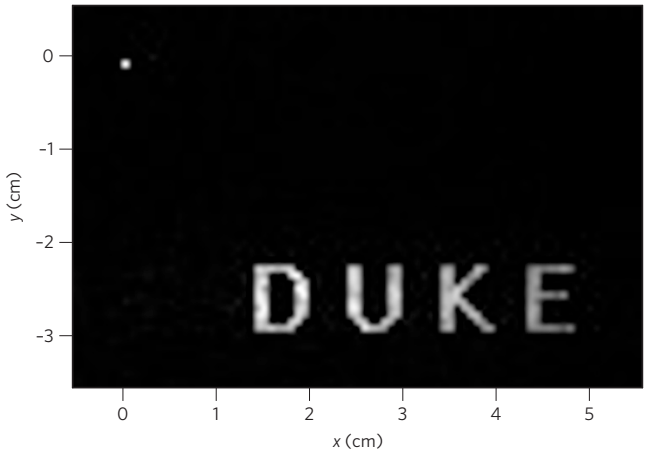

Figure 3 | Simulated image of the hologram at the focal plane of a lens. The focal length is 50.8 mm. Whereas the design considers a simple phase hologram, the simulation includes the effects of absorption and impedance mismatch creating an amplitude distribution. This decreases the efficiency of the hologram and creates artifacts such as the zeroth order beam visible in the top left corner (white box). See Supplementary Information for a more complete discussion.

values between 2.1 and 5.4, for an overall index contrast of 3.3. The effective absorption of the metamaterials was also retrieved, and is shown in the Supplementary Information. In a preliminary experiment[14], we have quantified the index contrast of a blazed diffraction grating fabricated using the same metamaterials and found an index contrast of 3.0, with excellent agreement between numerical simulations and measurements.

It should be noted that the metamaterial elements used in this work are anisotropic: their refractive index depends on the orientation of the electric field. The electric field is always applied along the long axis of the metamaterial elements, but because the sample has a graded index, the incident wave bends slightly and the electric field has small components along the other axes of the metamaterial. However, the hologram is thin; therefore, this effect is small and is neglected.

It should also be noted that the elements corresponding to the higher index values seem to show significant effective diamagnetic response (the relative permeability, μ_r, is as low as 0.8). This magnetic response does not derive from any intrinsic magnetic response of the structure, but rather is a known artefact arising from spatial dispersion[15]. Spatial dispersion arises when the wavelength of the light within the medium approaches the spacing of the elements. In this regime, the refractive index of the metamaterial is well defined, but not its wave impedance. Fortunately, we are designing a phase hologram, and the phase accumulation is mainly controlled by the effective index.

We designed a computer-generated phase hologram using the Gerchberg–Saxton iterative algorithm[16,17]—originally developed to retrieve phase information in electron microscopy, but now commonly used to design computer-generated holograms. This algorithm relies on the Fourier transform relationship between the complex transmittance of the hologram and the far-field image it generates, iteratively adjusting the constraints in the hologram and the image. Such computer-generated holograms can be experimentally realized in the Fraunhofer regime, when the image plane is located either in the far-field or at the focal plane of a lens.

The designed hologram, whose image is shown in Fig. 3, consists of the word 'DUKE'. The hologram consists of 150×150 pixels each consisting of 5×5 metamaterial elements. Each pixel consists of many elements because a significant component of the response of larger I-beams arises from the capacitive coupling between

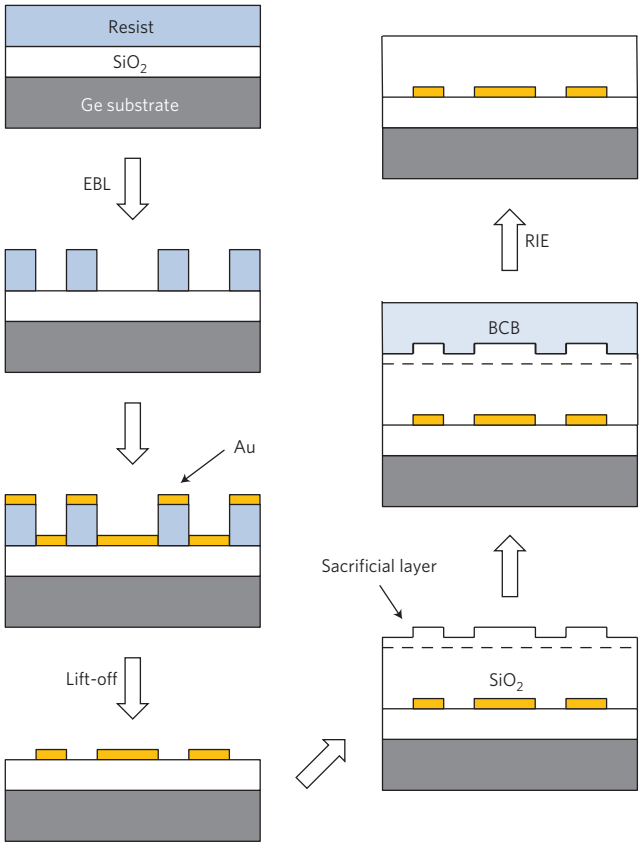

Figure 4 | Process flow for the fabrication of the multilayer metamaterial hologram. See text for details.

adjacent I-beam elements. Therefore, these elements must be surrounded by like elements to achieve the response that was simulated for an infinite array of elements. A simulation of the effect of the number of adjacent unit cells on the properties of a diffractive device is presented in the Supplementary Information. The total size of the hologram was chosen for fast writing in the electron-beam lithography instrument used to fabricate the metamaterial layers.

The process used to fabricate the hologram is illustrated in Fig. 4. The hologram was fabricated on a double-sided, polished germanium substrate ($\langle 100 \rangle$ oriented, undoped, $\rho > 40\,\Omega\,\mathrm{cm}$, $\sim 325\,\mu\mathrm{m}$ thick), which is transparent to infrared radiation at $10.6\,\mu\mathrm{m}$. A first 250-nm-thick SiO_2 layer was deposited on the Ge substrate by electron beam evaporation. A layer of resist was then spin-coated on the sample and electron-beam lithography (EBL, Elionix ELS-7500) used to pattern the hologram. A 3 nm chromium adhesion layer and a 75 nm gold layer were subsequently deposited by electron beam evaporation and lift-off was used to yield the metal structures of the first metamaterial layer, as well as alignment marks. The following 500-nm-thick SiO_2 layer was deposited in the same manner as the first, but a planarization step was necessary because evaporated films are fairly conformal. In the absence of planarization, subsequent EBL patterning was found to be unreliable because the topology of the SiO_2 films, which replicates that of the gold structures, interferes with the EBL exposure and the lift-off. To planarize the SiO_2 surface, a layer slightly thicker than necessary was deposited and a sacrificial benzocyclobutene (BCB) film (Dow Cyclotene 3022-35) was added, which has a planarizing effect. The BCB film and a controlled sacrificial portion of the SiO_2 film were then removed by reactive ion etching (RIE; CF_4 and O_2 chemistry) in conditions that were identified to remove BCB and SiO_2 at the same rate. The

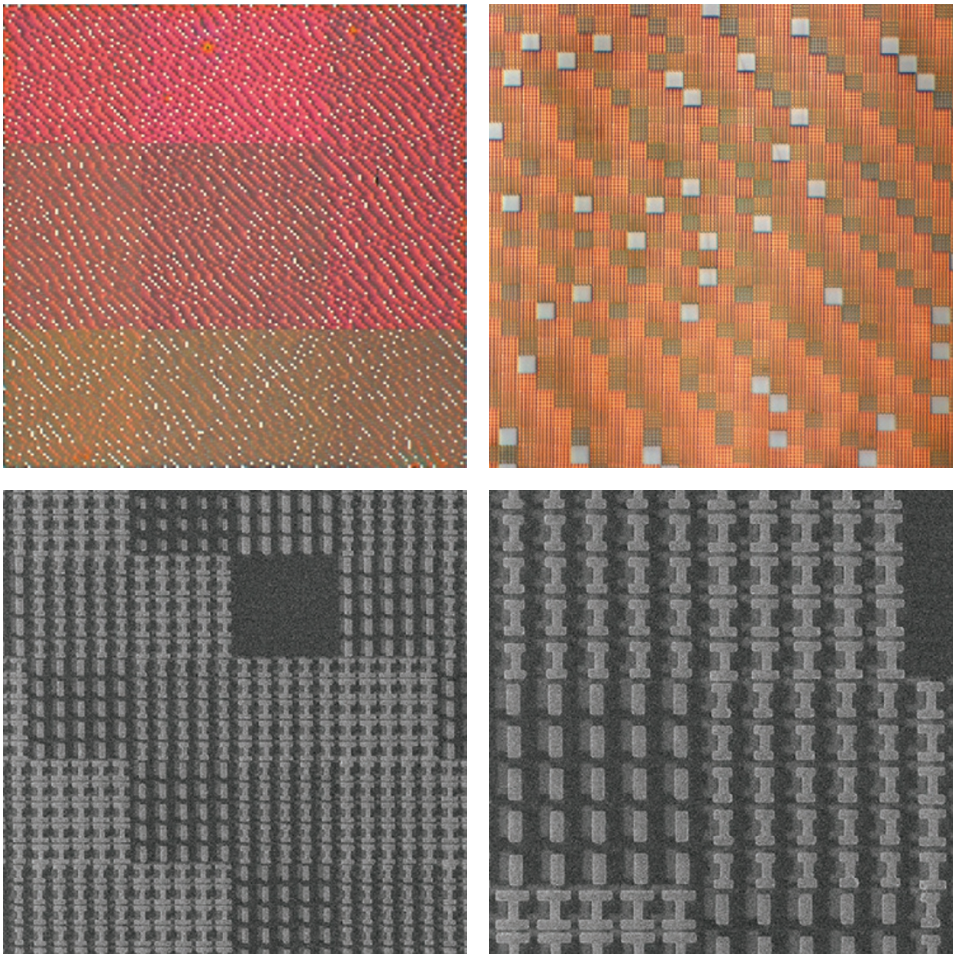

Figure 5 | Optical and SEM pictures of the hologram. The top left picture shows the whole 750 μm × 750 μm surface of the hologram. The top right picture shows a smaller region where individual 5 μm × 5 μm pixels are visible. The bottom left picture shows that pixels comprise 5 × 5 metamaterial elements on a 1 μm × 1 μm square grid. The bottom right picture is a closer view of a few pixels clearly showing ailgnment errors of about 200 nm between subsequent layers.

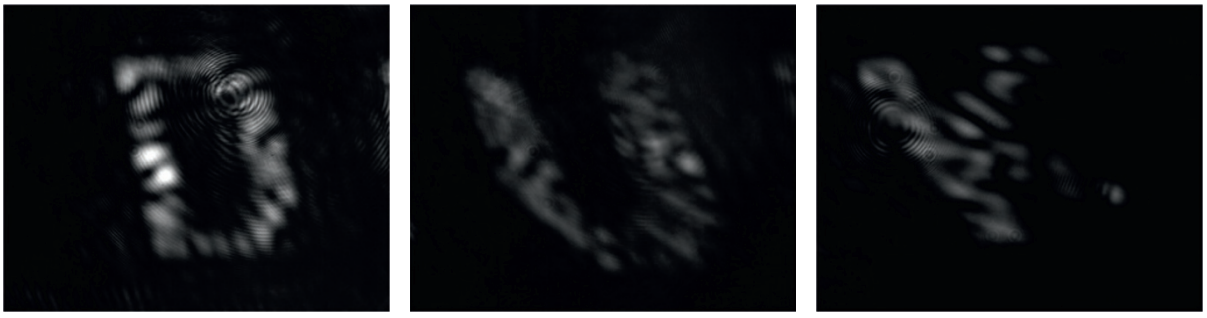

Figure 6 | Images generated by the hologram. The letters D, U and K are shown, the letter E was impossible to image with our set-up because it was too close to grazing incidence. A background image, taken without illumination, was subtracted from every image.

resulting SiO_2 surface was planar and suitable for further EBL patterning. Subsequent metal and SiO_2 layers were fabricated in the same manner until a three-metamaterial-layer sample was obtained. Alignment between the layers was controlled using the alignment marks, which were imaged at a magnification of ×100,000. The final SiO_2 layer, as the first one, is only 250 nm thick to preserve the symmetry of the dielectric environment around the metamaterial elements.

After fabrication, the sample was imaged using optical and SEM microscopy, as shown in Fig. 5. The images demonstrate the very regular size and positioning of the metallic elements. The dimensions of the metallic elements also reproduce faithfully the dimensions of the design. On the SEM images, alignment errors of around 200 nm between subsequent layers are evident. The coupling between subsequent layers does not play a significant role in the optical properties of the metamaterials used herein, and is therefore not of concern, but the boundaries of the pixels are not as well defined and this slightly reduces the diffraction efficiency of the hologram (see Supplementary Information).

We characterized the performance of the hologram using a system consisting of a CO_2 laser (Lasy3S, Access Laser Company), a linear polarizer, the hologram sample, a Ge lens with a 50.8 mm

focal length and an infrared camera (FLIR photon 640). The laser, the polarizer and the sample were collinear and the polarizer was rotated such that the electric field was parallel to the long axis of the rectangular elements and the I-beams. The lens and the camera were mounted on a rotating arm, allowing adjustment of the angle, and were positioned such that the camera was at the focal point of the lens.

The image generated by the hologram is shown in Fig. 6. Considering the size of the hologram and the dimensions of the camera's detector array, it was not possible to image all of the hologram in a single field-of-view, and the letters D, U and K were imaged separately. It was impossible to image the letter E, which was positioned too close to grazing incidence to be observed with our set-up.

Figure 6 shows proper reproduction of the designed hologram image, indicating that the index distribution on the hologram is close to the design. However, the contrast of the images is less than in the design. In addition to the aforementioned alignment errors, the fabricated hologram is composed of only three metamaterial layers whereas the designed hologram incorporates seven layers. The seven-layer-hologram results in an optimal 2π phase shift difference between lowest and highest refractive index regions. It should also be noted that the metamaterials used to realize the hologram have variable absorption, and reflect part of the light in a way that depends on the material impedance and refractive index, and the thickness of the hologram. Therefore, although the fabricated hologram provides the desired phase distribution, it also introduces an uncontrolled amplitude distribution. The modulation in amplitude does not affect the shape of the images in the image plane, but affects the diffraction efficiency. A study of the effect of the suboptimal phase shift, the absorption, the impedance mismatch and the misalignment is presented in the Supplementary Information. It was found that the most detrimental effects are suboptimal phase shift and absorption.

Although not demonstrated herein, it would be possible to include the amplitude modulation in the overall design. Recently, it has been suggested that metamaterials could be used to control both phase and amplitude in holograms[18].

The results reported herein demonstrate the fabrication of infrared optical devices with well-controlled arbitrary 2D refractive index distributions using 3D multilayer, metal-based metamaterials. The approach can be generalized to refractive index variations in three dimensions. However, thicker devices, potentially with many layers, will require metamaterials with lower absorption and planarizing dielectrics that can be implemented in three dimensions without difficulties such as cracking and delamination. In addition to holograms, the approach presented here easily extends to GRIN optical devices. If realized, full 3D arbitrary refractive index distributions will open the door to new devices combining diffraction, scattering and refraction[19].

The work presented here provides a glimpse of the opportunities available for advanced optical devices based on metamaterials, which can support quite complex material properties. In particular, the metamaterial structures used here can readily be configured to manage polarization, so that controlled anisotropy or even chirality could be introduced to the metamaterial, providing more degrees of control without an extra burden on the fabrication. Finally, a 3D medium whose optical properties can be controlled point-by-point may ultimately serve as a platform for transformation optical media, with unprecedented optical functionality.

Received 27 October 2011; accepted 13 February 2012; published online 18 March 2012

References

1. Gordon, J. M. Spherical gradient-index lenses as perfect imaging and maximum power transfer devices. *Appl. Opt.* **39,** 3825–3832 (2000).
2. Pendry, J. B., Schurig, D. & Smith, D. R. Controlling electromagnetic fields. *Science* **312,** 1780–1782 (2006).
3. Schurig, D. *et al.* Metamaterial electromagnetic cloak at microwave frequencies. *Science* **314,** 977–980 (2006).
4. Dobrowolski, J. A. in *Handbook of Optics* 2nd edn, Vol. 1 (eds Bass, M. & Stryland, E. W. V.) Ch. 42 (McGraw Hill, 1995).
5. Yakhkind, A. K. Optical graded-index elements made from glass. *Optic. Zh.* **70,** 54–60 (2003) *J. Opt. Technol.* **70** 877–881 (2003) (transl.).
6. Jin, Y., Tai, H., Hiltner, A., Baer, E. & Shirk, J. S. New class of bioinspired lenses with a gradient refractive index. *J. Appl. Polym. Sci.* **103,** 1834–1841 (2007).
7. Glezer, E. N. *et al.* Three-dimensional optical storage inside transparent materials. *Opt. Lett.* **21,** 2023–2025 (1996).
8. Freese, W., Kämpfe, T., Kley, E-B. & Tünnermann, A. Design of binary subwavelength multiphase level computer generated holograms. *Opt. Lett.* **35,** 676–678 (2010).
9. Levy, U., Kim, H-C., Tsai, C-H. & Fainman, Y. Near-infrared demonstration of computer generated holograms implemented by using subwavelength gratings with space-variant orientation. *Opt. Lett.* **30,** 2089–2091 (2005).
10. Choi, M. *et al.* A terahertz metamaterial with unnaturally high refractive index. *Nature* **470,** 369–374 (2011).
11. Smith, D. R., Schultz, S., Markoš, P. & Soukoulis, C. M. Determination of effective permittivity and permeability of metamaterials from reflection and transmission coefficients. *Phys. Rev. B* **65,** 195104 (2002).
12. Ordal, M. A. *et al.* Optical properties of the metals Al, Co, Cu, Au, Fe, Pb, Ni, Pd, Pt, Ag, Ti, and W in the infrared and far infrared. *Appl. Opt.* **22,** 1099–1119 (1983).
13. Lovrinčić, R. & Pucci, A. Infrared optical properties of chromium nanoscale films with a phase transition. *Phys. Rev. B* **80,** 205404 (2009).
14. Tsai, Y-J. *et al.* Design and fabrication of a metamaterial gradient index diffraction grating at infrared wavelengths. *Opt. Express* **19,** 24411–24423 (2011).
15. Smith, D. R. Analytic expressions for the constitutive parameters of magnetoelectric metamaterials. *Phys. Rev. E* **81,** 036605 (2010).
16. Gerchberg, R. W. & Saxton, W. O. A practical algorithm for the determination of phase from image and diffraction plane pictures. *Optik* **35,** 237–246 (1972).
17. Wyrowski, F. Design theory of diffractive elements in the paraxial domain. *J. Opt. Soc. Am. A* **10,** 1553–1561 (1993).
18. Walther, B., Helgert, C., Rockstuhl, C. & Pertsch, T. Diffractive optical elements based on plasmonic metamaterials. *Appl. Phys. Lett.* **98,** 191101 (2011).
19. Gerke, T. D. & Piestun, R. Aperiodic volume optics. *Nature Photon.* **4,** 188–193 (2010).

Acknowledgements

This work was supported by a Multidisciplinary University Research Initiative, sponsored by the US Army Research Office (Grant No. W911NF-09-1-0539).

Author contributions

S.L., Y-J.T. and D.R.S. conceived the application of metamaterials for holography and designed the experiment. T.T. and N.M.J. developed the fabrication protocols. Y-J.T. carried out simulations and characterization. T.T. fabricated the sample. S.L. wrote the manuscript.

Additional information

The authors declare no competing financial interests. Supplementary information accompanies this paper on www.nature.com/naturematerials. Reprints and permissions information is available online at www.nature.com/reprints. Correspondence and requests for materials should be addressed to S.L. or D.R.S.